San L.Tolentino

Research
National Experimental Polytechnic
University"AJS" (UNEXPO)
Bolívar
Venezuela

Research collaborator
Group of Mathematical Modeling and
Numerical Simulation (GMMNS)
National University of Engineering (UNI)
Lima
Perú

Jorge Mírez

Elec. Mech, Eng.; MSc & Dr Physics
Professor
Group of Mathematical Modeling and
Numerical Simulation (GMMNS)
National University of Engineering (UNI)
Lima
Perú

Simón A. Caraballo

Professor
UNEXPO Polytechnic University
Department of Mechanical Engineering
Bolívar
Venezuela

Numerical Analysis of the Shock Train in Conical Nozzles with Straight-Cut Throats

The overexpanded flow regime in supersonic rocket engine nozzles presents different shock wave structures due to the geometrical configurations of the internal walls. In the present investigation, the study of the shock train phenomenon is addressed for a group of convergent-divergent conical nozzles with straight-cut throats for the overexpanded flow condition for NPR=12. The viscous and compressible flow field under stationary conditions is simulated with the RANS model in the ANSYS-Fluent R16.2 code, which applies the finite volume method (FVM) to discretize the computational domain. The Spalart-Allmaras turbulence model is used, and Sutherland's law is used for the viscosity as a function of temperature. The results show that, in the straight-cut throat section, as its length increases, the flow accelerates and decelerates with the presence of oblique shocks, which forms a definite shock train structure, where the flow velocity fluctuations are within the estimated Mach number range of 0.6 to 1.8. Increasing the throat length significantly affects the flow development at the nozzle outlet, which decreases the thrust force.

Keywords: Conical nozzle, Oblique shock, Overexpanded flow, Straight-cut throat, Shock train, Velocity fluctuation

1. INTRODUCTION

The viscous and compressible flow field regime at super–sonic velocity is recurrently studied in diffusers, ejectors, shock tubes, ducts, scramjet, and ramjet [-3], as well as in supersonic nozzles with different geometries applied to the aerospace area [3,4]. The geometries of the internal walls of such devices condition the flow transit so that in dif–ferent regions of the flow, there are variations in velocity, pressure, and temperature, among other thermodynamic parameters.

In the compressible flow regime in straight or slightly diverging duct sections, the propagation of oblique waves has a trajectory based on the inlet and outlet pressure, and the whole wave propagation is called a shock train [1,5,6].

On the other hand, the compressible flow regime in convergent-divergent supersonic nozzles, such as planar, bell, parabolic, or other divergent geometries, depending on the nozzle inlet pressure and outlet pre–ssure conditions, the flow condition can be overex–panded, equalized or under expanded [3,7].

In the case of overexpanded flow, the shock wave conditions occur at divergence or downstream after nozzle exit. The thrust force is conditioned by the deve–lopment of the flow regime leaving the nozzle [3,7].

The normal, oblique, and reflected shock waves inte–ract with the turbulent boundary layer in the flow regions adjacent to the walls, which causes instability in the position of the normal shock front. In the region of the flow with a shock wave, before the shock, the velocity is supersonic, and after the shock, the velocity is subsonic, and the pressure and temperature gradients undergo abrupt jumps in that region of the shock. In turbulent flow, the effect of friction and wall temperature, vortices, restricted shock separation (RSS), and free shock separation (FSS) are present [8-12]. Flow fluctuations in the presence of shock waves cause variations of lateral pressure loads on the walls [9,11,13]. The Mach disk at the nozzle outlet is affected by radial pressure gradients [14], and in the plume, triple shock wave configurations are present [15]. Prandtl-Meyer expansion waves are also present at the wall edge at the nozzle exit [7,8].

Within the extension of the group of conventional supersonic nozzles are the conical nozzles with straight-cut throats, which have applications in solid fuel rocket engines, either sounding rockets or amateur category rockets [16]. The rocket engine is a single body com–posed of a combustion chamber and a nozzle, and its dimensions vary depending on the power required to generate rocket thrust. It should be noted that the throat section of the nozzle is a straight tube section of pa–rameterized length L_g/D_g, where L_g is its length, and D_g is its diameter. For reference, some rocket engines re–ported by Rogers [16] that have employed conical nozzles with straight-cut throat are mentioned, such as the TU-223 Mace Booster of length 3.27 m and conical nozzle with $L_g/D_g = 0.303$; the TE-M-416 Tomahawk of length 5.10 m and conical nozzle with $L_g/D_g = 0.5$., and the TE-M-388 Iroquois of length 2.65 m and conical nozzle with $L_g/D_g = 0.952$.

Also mentioned is the solid fuel engine sounding rockets manufactured by the University of Los Andes (ULA) of Venezuela, within the framework of activities carried out by the Rectoral Commission of the Space

Sciences Program and the Center for Atmospheric and Space Research (CIAE-ULA) [17]. The rocket engines use conical nozzles with straight-cut throats, which have undergone performance testing. The rockets have also undergone continuous improvements in flight perfor–mance, thrust, and parabolic-typeballistic trajectory. The solid fuel used in the engines combines potassium nitrate as an oxidizer (65% mass) and sucrose as fuel (35% mass). Fig. 1 shows a group of supersonic nozzles from the ULA series of sounding rockets [17].

Figure 1. Sounding rockets of the ULA series [17] using conical nozzles with straight-cut throats.

Figure 2(a) illustrates a basic schematic of the struc–ture of the shock train in the straight-cut throat of a convergent-divergent nozzle, where the shock train is composed of oblique, reflected, and Mach disk shocks. Fig. 2(b) illustrates a schematic of the normal shock front (Mach disk) and the oblique and reflected shock waves occurring in the divergent section for the over–expanded flow condition.

Figure 3 illustrates images of shock wave structures captured with the Schlieren technique during laboratory experiments. Fig.3 (a) shows a configuration of the shock train in a duct with parallel walls reported by Geerts and Yu [18], where the oblique shocks form a sequence of diamonds. Fig. 3(b) shows the shock train in a divergent duct reported by Weiss et al. [19]; as the wave propagates, its intensity decreases downstream. Likewise, in double divergent nozzles [20], for very narrow divergent angles, wave propagation is present. Fig.3(c) illustrates the structure of the shock in the divergent of a planar nozzle reported by Hunter [13] for the overexpanded flow condition, in which the oblique, reflected, and normal shock front caused by flow braking is observed.

Different authors have addressed experimental studies on parallel-walled ducts. In them, the pressures in the flow region adjacent to the duct walls present instabilities that are caused by the shock train, and the intensity of the flow fluctuation decreases downstream with pressure increases [1,5,18,21]. According to the case of self-excited oscillation and forced oscillation, the asymmetric characteristics of the first shock wave are negatively correlated with the shock velocity [22, ,23]. The wall

temperature also influences the pressure distribution in the shock train [24]. In the case of a diverging duct with a normal suction slot, when the flow passes through the diverging duct, the pressure gradient across the primary shock affects the boundary layer of the flow region adjacent to the wall across the suction slot [19].
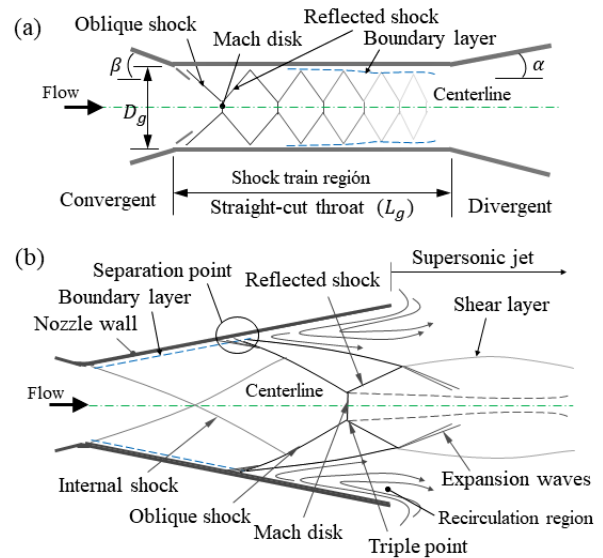

Figure 2. Basic schematic illustrating the structure of the flow regime behavior in a throat length nozzle. (a) Throat length section. (b) Divergent section.
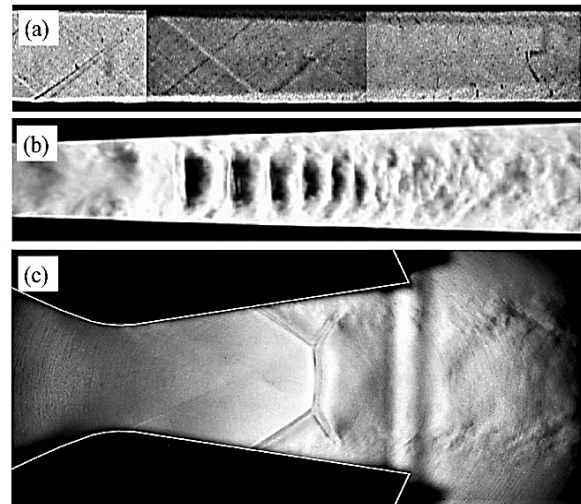

Figure 3. Shock waveform structures captured with the Schlieren technique (a) Shock train in a parallel-walled duct [17] (b) Shock train in a diverging duct [18] (c) Shock waves in the divergence of a planar nozzle [13].

Regarding convergent-divergent nozzles with straight-cut throats, flow behavior studies have been reported applying CFD computational tools [25,25].

For flow in planar nozzles with straight-cut throat and for the half angle of the divergent $\alpha = 11.01°$, Tolentino et al. [27] reported a shock train. The study was approached for progressive increments of the straight-cut throat up to $L_t/h_t = 1.5$, where L_t is the straight-cut throat length, and h_t is the throat height. The flow exhibited velocity fluctuations in the estimated range of Mach 1 to Mach 1.2.

While, for flow in conical nozzles with straight-cut throat and $\alpha = 10°$, Tolentino and Mirez [28] reported for throat length increments up to $L_g/D_g = 2$ velocity

fluctuations in the estimated range from Mach 0.65 to Mach 1.74. It is worth noting that when comparing the flow behavior of the throat section between a conical nozzle and a planar nozzle, which has been presented above, the conical nozzle presents greater flow fluctu–ation. Other studies performed applying CFD for flow simulation in conical nozzles with straight-cut throat $L_g/D_g \approx 1$ [29-31] have reported that velocity fluctu–ations with the presence of oblique shocks are present in the throat section.

The analysis of the flow behavior in a straight-cut throat nozzle has two sections to take into account: the throat section and the divergent section. The throat length conditions the flow behavior in the divergent for the over–expanded flow condition. Therefore, based on the research reports mentioned above, the research on the flow behavior in conical nozzles with straight-cut throats has been moti–vated to continue.

In the present work, the object of study is to analyze the compressible flow behavior for different throat section lengths of a group of convergent-divergent conical nozzles and to determine the effect that throat length has on the flow development in the throat section and at the nozzle outlet. The flow is simulated in computational domains by applying CFD, for which the ANSYS-Fluent R16.2 code is used to achieve the proposed objective. Section 3 presents the results and discussions. Section 4 presents the conclusions.

2. MATERIALS VAND METHODS

2.1 Computational domain and meshing

The geometry of the conical nozzle with straight-cut throat, L_g/D_g, considered for the study of viscous and compressible flow is illustrated in Fig. 4(a), as well as the boundary conditions applied to the computational domain are indicated there. Fig. 4(b) illustrates the meshed computational domain, as well as details of the meshing of the throat section (Fig. 4(c) and 4(d)).

The conical nozzle is designed for isentropic flow for air parameters $k = 1.4$, for Mach 3.33 and area ratio $A_e/A^* = 5.811$, where A_e is the area at the nozzle exit and A^* is the throat area. As well as, the half angle of the divergent $\alpha = 10°$ was taken into account, which is within the classification of off-design supersonic nozzles, $\alpha < 12°$.

For the flow field simulations, the throat diameter $D_g = 0.02$ m was taken into account for five cases of throat lengths: $L_g/D_g = 0.05$, $L_g/D_g = 0.15$, $L_g/D_g = 0.45$, $L_g/D_g = 1$, and $L_g/D_g = 2$. The length of the convergent is Lc = 1.5 D_g, and of the divergent is $L_c = 4D_g$. The half angle of the convergent is $\beta = 30°$ and of the divergent is $\alpha = 10°$. The longitudinal dimensions of the nozzle section are presented in Table 1.

Table 1. Longitudinal dimensions of the conical nozzle geometry with throat length

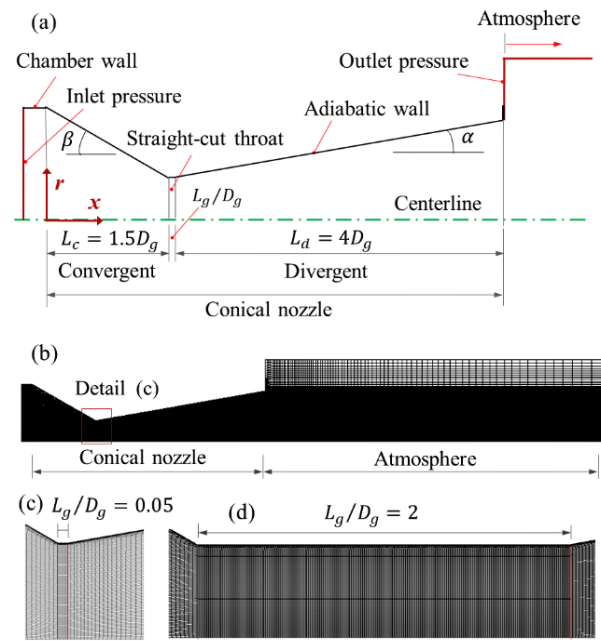| L_g/D_g	Nozzle cross-section range: position x/D_g		
	Convergent	Straight-cutthroat	Divergent
0.05	0 – 1.5	1.5 – 1.55	1.55 – 5.55
0.15	0 – 1.5	1.5 – 1.65	1.65 – 5.65
0.45	0 – 1.5	1.5 – 1.95	1.95 – 5.95
1	0 – 1.5	1.5 – 2.5	2.5 – 6.5
2	0 – 1.5	1.5 – 3.5	3.5 – 7.5

Figure 4. Basic schematic of the geometry of the convergent-divergent conical nozzle with straight-cut throat. (a) Computational domain, in which the boundary conditions are indicated. (b) the Meshed domain of the nozzle and a region of the atmosphere, for a total of 30813 elements. (c) Meshed detail of straight-cut throat section.

From the total computational domain, a section of the combustion chamber domain was taken into account to direct the flow at the inlet of the convergent section, with a length of $0.25D_g$. For the flow to the atmosphere discharge, a domain section with a horizontal length of $8D_g$ and a vertical length of $1.955D_g$ was taken into account, respectively.

The computational domain of the conical nozzle was considered in 2D because of its symmetry with respect to the x-axis. The boundary conditions (Fig. 4(a)) applied to the nozzle inslet are stagnation pressure $p_0 = 1200$ kPa and stagnation temperature $T_0 = 1620$ K, and for the ambient region of the atmosphere are pressure $p = 100$ kPa and temperature $T = 300$ K. For which we have a nozzle pressure ratio NPR = 12, where NPR = p_0/p.

The flow velocity is zero in the adiabatic wall due to the no-slip condition. In axial symmetry, the flow velocity in the radial direction is zero. The gravity effect of the flow discharge in the atmosphere was not taken into account, so there is no convective effect due to the density difference due to temperature variations since the computational domain is 2D with axial symmetry.

The domain meshing was performed in the ANSYS-Meshing Platform, using ICEM-CFD interaction to discretize the domain. The meshed domain with 30813 elements for $L_g/D_g = 0.05$ is illustrated in Fig.4(b), and an enlarged detail of the throat section is shown in Fig.4(c), where the mesh of the throat length section has 500 elements. Also shown for the throat section meshing is the detail for $L_g/D_g = 2$ in Fig.4(d), which has 20000 elements. It should be noted the meshing for other throat sections, for the cases $L_g/D_g = 0.15$ (1500 elements), $L_g/D_g = 0.45$ (4500 elements), and $L_g/D_g = 1$ (10000 elements) is not presented in Fig.4.

2.2 Governing equations

For the simulation of the compressible viscous flow field, Reynolds-Averaged Navier-Stokes (RANS) equa–tions were used for steady-state conditions. The computational simulation code used was ANSYS-Fluent R16.2, which applies the finite volume method (FVM) [25,26,32].

Equation (1) of the conservation of mass, equation (2) of momentum in a fluid, equation (3) of energy, and equation (4) of state of the ideal gas [25,26,32]. These equations, without considering the time variable, in the compact form are expressed as:

$$\nabla \cdot \left(\rho u_i \right) = 0 \tag{1}$$

where ρ is the density, and u is the flow velocity.

$$p = \rho R T \quad {}^{\wedge} \tag{2}$$

where, p is the pressure, $\overline{\overline{\tau}}$ is the stress tensor, and $-\overline{\rho u_i' u_j'}$ is the Reynolds stress.

$$\nabla \cdot \left(u_i \left(\rho E + p \right) \right) = \nabla \cdot \left(k_{eff} \nabla T + \left(\overline{\overline{\tau}}_{eff} u_i \right) \right) \tag{3}$$

where, E is the total energy, k_{eff} is the effective thermal conductivity, T is the temperature, and $\overline{\overline{\tau}}_{eff}$ is the effec–tive stress tensor.

$$p = \rho R T \tag{4}$$

where R is the gas constant.

For turbulence modeling of the compressible flow, the Spalart-Allmaras turbulence model [33] was used, and for flow viscosity as a function of temperature, Suhterland's law equation [34] was used.

For compressible flow, the Mach number, M, is classified in the following ranges: (a) subsonic flow $0.3 \leq M \leq 0.8$; transonic flow $0.8 \leq M \leq 1.2$; supersonic flow $1.2 \leq M \leq 5$; hypersonic flow $M > 5$ [7]. For incompressible flow consideration, we have $M < 0.3$.

The flow in the nozzle is considered as an ideal gas, as an approximate behavior to air, the flow parameters being as follows: specific heat ratio $k = 1.4$, specific heat at constant pressure $C_p = 1006.43$ J/(kg·K), thermal conductivity $k_t = 0.042$ W/(m·K), and gas constant $R = 287$ J/(kg·K) [31].

2.3 Computational solution method

Different options were considered for the computational solution method in the ANSYS-Fluent R16.2 code. Flow type: density-based. Time: steady. 2D space: axisym–metric. Formulation: implicit. Flux type: Roe-FDS. Gradi–ent: Least squares cell based. Flow: second-order upwind. Modified turbulent viscosity: second-order upwind. Initi–alization methods: hybrid. For the control of the residual monitor, 1×10^{-6} was taken into account for continuity, speed, and energy. The simulations were in the range of a number of iterations: 26,000 to 87,000.

The computer equipment used has the following characteristics: Dell CPU, model Optiplex 7010, i5 3470, four processors of 3.2 GHz, and 8 Gb of RAM.

2.4 Numerical convergence analysis

For the numerical convergence analysis, three meshes of the computational domain were performed for the conical nozzle with straight-cut throat $L_g/D_g = 0.05$, being refined the mesh for the regions adjacent to the walls of the nozzle due to the presence of shear forces in the flow development. Being for mesh 1 with 30809 elements, mesh 2 with 31110 elements, and mesh 3 with 32121 elements. The flow was simulated for NPR = 12 with the Spalart-Allmaras turbulence model [33].

The results of y^+ in shear stress value for the three cases of 2D computational domain meshing are illus–trated in Fig.5, which shows two peaks, a first peak at position $x/D_g = 1.5$ for $y^+ < 19$; the other peak occurs at the exit of the nozzle, at position $x/D_g = 5.55$ for $y^+ < 23$.

The three y^+ curves are overlapping, which shows that for further increments of the mesh density, they do not have a significant contribution; therefore, mesh 1 with 30809 elements (Fig.4(b)) is satisfactory for the flow field simulation. The results of the numerical si–mulations of the obtained mass flow of 0.355 kg/s were also compared with the mass flow for isentropic flow of 0.378 kg/s, which had an absolute error of 0.023.
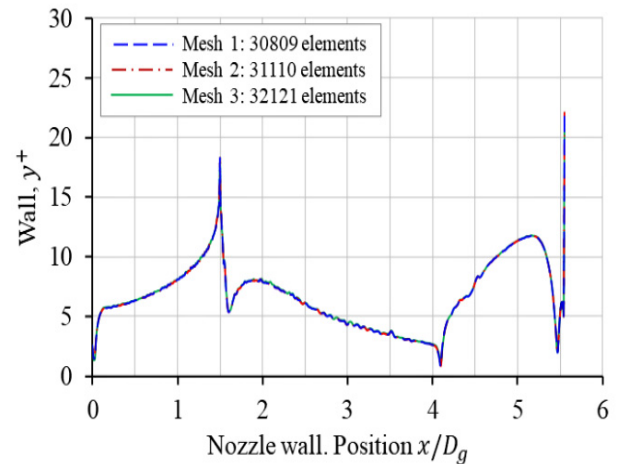

Figure 5. Curve trajectories of y^+ at the shear stress value evaluated at the adiabatic wall of the conical nozzle for flow with NPR = 12.

2.5 Validation of the Spalart-Allmaras turbulence model

The Spalart-Allmaras turbulence model [33] is a one-equation model that has good answers for adverse pressure gradients and boundary layer separation, which was validated with experimental flow pressure data at the walls of a convergent-divergent planar nozzle from the work of Hunter [13] for NPR=3.413. Likewise, the Spalart-Allmaras turbulence model [33] was compared with the SST k - ω turbulence model of Menter [35], standard k - ω of Wilcox [36], and RSM of Launder et al. [37], as shown in Fig. 6, where the range of the convergent is located at $0 \leq x/x_t \leq 1$ and of the divergent at $1 \leq x/x_t \leq 2$. The best curve fit is presented for the Spalart-Allmaras S-A turbulence model, where at position $x/x_t = 1.717$, the lowest pressure drops with an error of 0.32% are presented. The error is greater than 1.68% for the other three turbulence models.
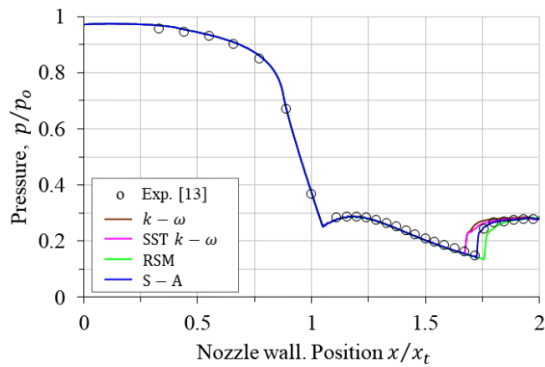
Figure 6. Comparison of curve fits of four turbulence models with experimental pressure data [13] evaluated at the nozzle wall for flow with NPR = 3.413.

3. RESULTS AND DISCUSSION

3.1 Mach number flow patterns

The simulations of the overexpanded flow field for the five straight-cut throat study cases $L_g/D_g = 0.05$, $L_g/D_g = 0.15$, $L_g/D_g = 0.45$, $L_g/D_g = 1$, and $L_g/D_g = 2$ are shown in Fig.7, where the red region presents the Mach number gradient and the blue region with lower magnitude. In the divergent, oblique shock waves and flow separation occur. In the region of the atmosphere, the supersonic jet is discharged, whereas in the central region, the plume is formed. Likewise, normal shock waves are present in the atmosphere adjacent to the nozzle's exit.
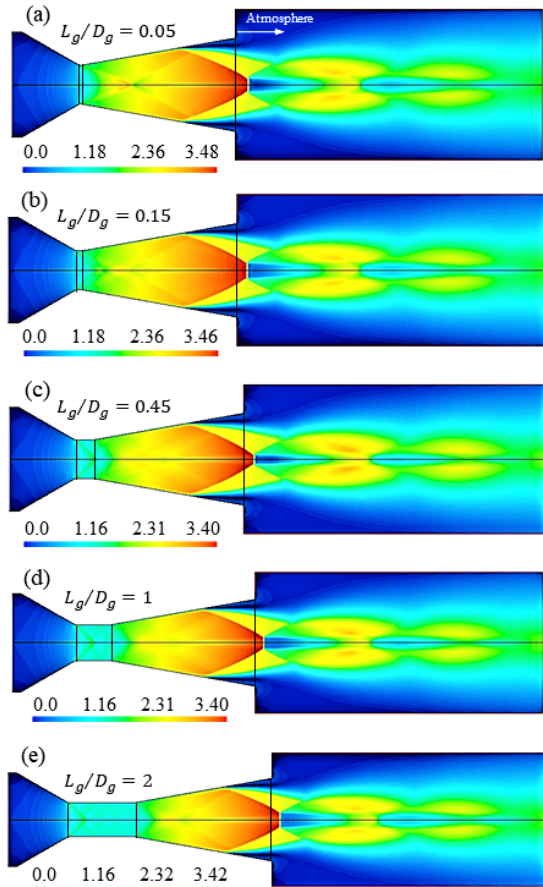

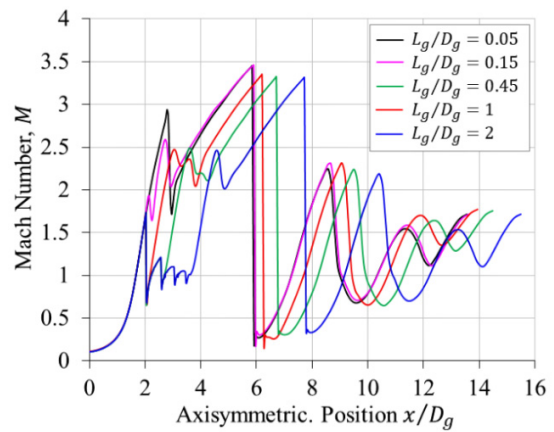**Figure 7. Mach number flow field for five cases of straight-cut throat increments.**

Figure 8. Mach number patterns evaluated in axial symmetry correspond to the flow field in Fig.7.

Figure 8 illustrates the behavioral patterns of the Mach number curve trajectories evaluated in axial sym–metry in the nozzle section and in the atmosphere re–gion, corresponding to Fig. 7 of the Mach number field. As the throat length increases, velocity fluctu–ations are presented in that section, whereby the flow velocity at the nozzle exit is affected, where the variations of the flow velocity with respect to Mach number at the nozzle exit are presented in Table 2, being the largest values for $L_g/D_g = 0.05$ and $L_g/D_g = 0.15$.

Likewise, for the flow at the nozzle outlet, evaluated in the radial direction, the behavior of the Mach number pattern curves is illustrated in Fig.9, where the central region ($0 \leq r/R_g \leq 1$) presents higher velocity with a step jump in the estimated range of 2.25 M $M < 3.4$, where the separation between curves is due to the effect of throat length, whereas, for the flow region close to the wall ($1 \leq r/R_g \leq 1.75$) the velocity decreases and the effect of throat length is with less intensity. Likewise, for the flow velocity adjacent to the wall, the flow velocity is subsonic less than Mach 0.8 ($1.75 \leq r/R_g \leq 2.410$).

Table 2. Mach number values at the nozzle outlet, evaluated in axial symmetry.

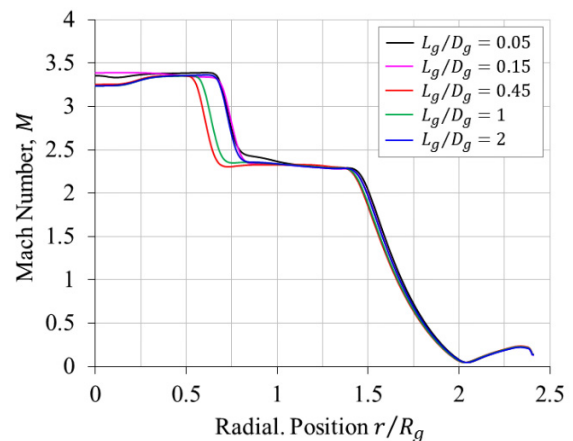| Straight-cut throat L_g/D_g	Position x/D_g	Mach number M
0.05	5.55	3.353
0.15	5.65	3.383
0.45	5.95	3.253

Figure 9. Mach number patterns were evaluated in the radial direction at the nozzle outlet, corresponding to the flow field in Fig. 7.

3.1.1 Shock train in the throat section

The formation structure of the shock train in the straight-cut throat, for $L_g/D_g = 0.05$, $L_g/D_g = 0.15$, $L_g/D_g = 0.45$, $L_g/D_g = 1$ and $L_g/D_g = 2$ are shown in Fig.10 in grayscale, which was evaluated for the density field, and is related to the throat section evaluated for the Mach number field shown above in Fig. 7. It is observed that as the length L_g increases, internal shocks composed of oblique and reflected shocks are generated. Likewise, in the throat section, the velocity fluctuations evaluated from the central region and towards the nozzle walls are shown in Fig. 11, where the flow accelerates and decelerates in different regions as a consequence of the internal shocks.

For the range of $0.05 \leq L_g/D_g \leq 0.15$, there is no flow disturbance with the presence of a shock train (Fig. 10(a), 11(a), 10(b), and 11(b), whereas for $L_g/D_g = 0.45$ (Fig. 10(c) and 11(c)), the oblique shock is present in the throat section with higher intensity. For $L_g/D_g = 1$ (Fig. 10(d) and 11(d)), oblique and reflected shocks are present, and a normal shock front is present in the estimated range of $0.65 < M$ 1.74.

For $L_g/D_g = 2$ (Fig. 10(e) and 11(e)), the propagation of the internal shocks increases and decreases in intensity as they travel toward the throat exit. It is evident that, in the throat section adjacent to the inlet, the normal shock front is present, with regions of the flow at subsonic, transonic, and supersonic velocity, while, for the region of the flow near the throat exit, it reaches transonic velocity.
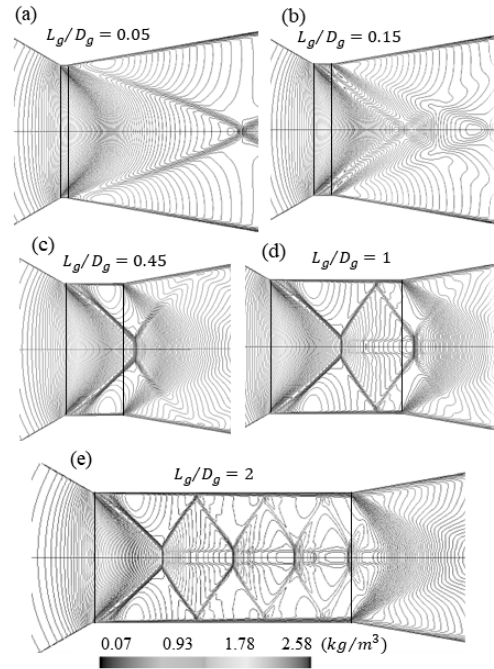

Figure 10. Density flow field. Structure of the shock train formation in the throat section.
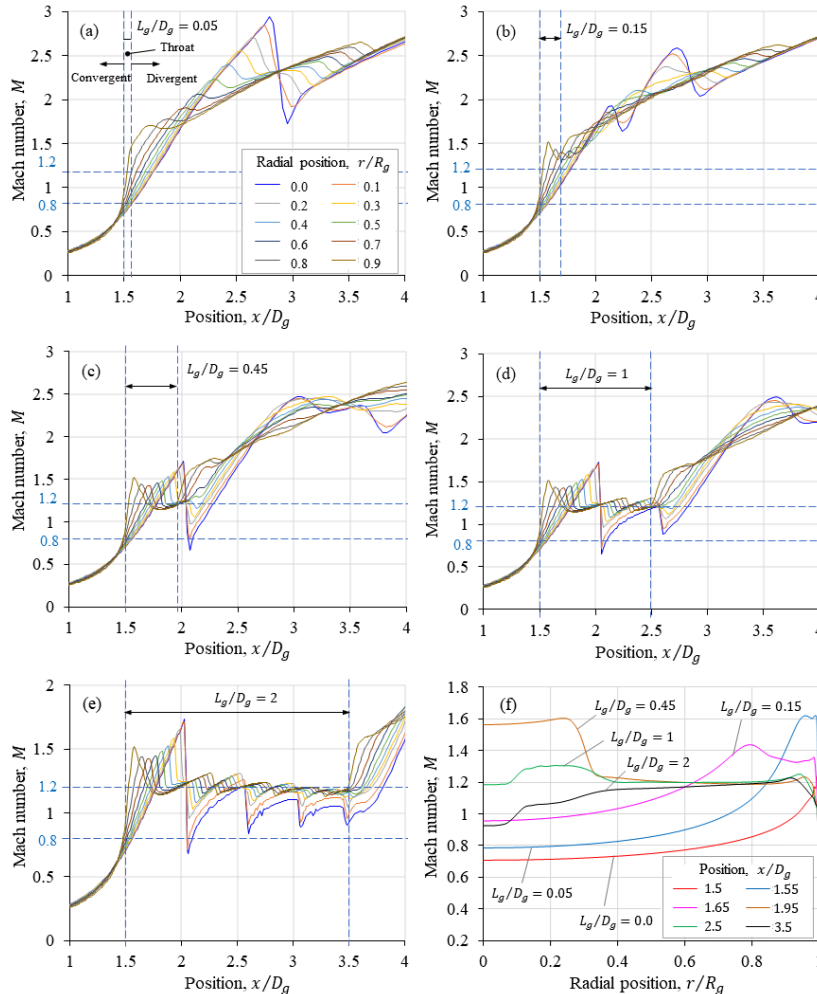

Figure 11. Flow fluctuations at throat section: (a) 1.5 ≤ x/D_g ≤ 1.55, (b) 1.5 ≤ x/D_g ≤ 1.65, (c) 1.5 ≤ x/D_g ≤ 1.95, (d) 1.5 ≤ x/D_g ≤ 2.5, (e) 1.5 ≤ x/D_g ≤ 3.5. (f) Mach number at throat exit, position x/D_g.

The Mach number curve trajectories at the throat exit, in the radial direction, r/R_g, are shown in Fig. 11(f), where R_g is the throat radius. For additional reference, the curve for $L_g/D_g = 0$, where the central region of the flow is close to Mach 0.7, has been included, whereas the other curves, for $L_g/D_g = 0.05,$, are close to Mach 0.8, and for $L_g/D_g = 0.15$, , close to Mach 1. The flow region adjacent to the wall is larger than Mach 1 for these three curves. In contrast, for the other curves in the central region of the flow, one has that for $L_g/D_g = 0.45,$, the velocity is around Mach 1.6, for $L_g/D_g = 1$, the velocity is around Mach 1.2, and for $L_g/D_g = 2$, the velocity is around Mach 1.

It is evidenced that the conical nozzles with straight-cut throat $L_g/D_g = 0.45$ $L_g/D_g = 1$, and $L_g/D_g = 2$, contribute to increasing flow fluctuations in that section; therefore, the shock train is present (Fig.10). These velocity fluctuations originating from the throat section affect the flow at the nozzle outlet (Fig.9); therefore, the thrust force must also exhibit variations in magnitude as the throat length increases from $L_g/D_g = 0.05$, to $L_g/D_g = 2$.

Similar results of flow velocity fluctuations with the presence of normal shock front in straight-cut throat section in conical nozzles have been reported for mean divergent angles $\alpha = 9°$ [30], $\alpha = 10°$ [28], and $\alpha = 11°$ [29,30], which report that throat length significantly affects in the development of flow regime in the throat and divergent section. Flow velocity fluctuations have also been reported in planar nozzles with straight-cut throats, where the shock train exhibits transonic velocity variations in the Mach number range from 1 to 1.2 [27].

The following section presents the analysis of the effect of increasing the throat length on the flow development at the nozzle outlet.

3.1.2 Effect of throat length on flow development at the nozzle outlet

Table 3 presents the average values of the viscous flow parameters obtained in the radial direction at the nozzle outlet for the flow with NPR = 12 and mass flow 0.355 kg/s. The plots of the curves for the pressure ratios p_i/p_e, velocity v_i/v_e, temperature T_i/T_e, Mach number M_i/M_e, and thrust force F_i/F_e, for the range of $0.05 \leq L_g/D_g \leq 2$ are shown in Fig. 12. It should be noted that subscript e corresponds to viscous flow, and subscript i for isentropic flow. In addition, the data for $L_g/D_g = 0.05$ (Table 3) was taken into consideration as a standard basis to obtain dimensionless parameters.

It is observed in Fig. 12 that for $0.05 \leq L_g/D_g \leq 0.15$ (range 1), the intercept of the curve, there the thrust force, and velocity have higher magnitude; therefore, it is an optimum range of throat length for better performance of the off-design conical nozzle, pointing out that, in such range, no internal shocks occur for $0.15 \leq L_g/D_g \leq 0.35$ (range 2), the thrust force and velocity decrease in magnitude. For $0.35 \leq L_g/D_g \leq 2$ (range 3), they slightly increase in magnitude but are below the values with respect to $0.15 \leq L_g/D_g \leq 0.35$; and for these two ranges, the velocity fluctuations are due to the presence of internal shocks.

Table 4 presents the values of standard deviation and coefficient of variation for ranges 1, 2, and 3 with respect to the pressure, velocity, temperature, Mach number, and thrust force ratios. Where the standard deviation is below 0.1% and the coefficient of variation is less than 3%. For $0.05 \leq L_g/D_g \leq 0.15$ (range 1), the coefficient of variation less than 1% was obtained.

Table 3: Average values of thermodynamic parameters for viscous flow evaluated at the nozzle outlet for throat length $L_g/D_g = 0.05$.

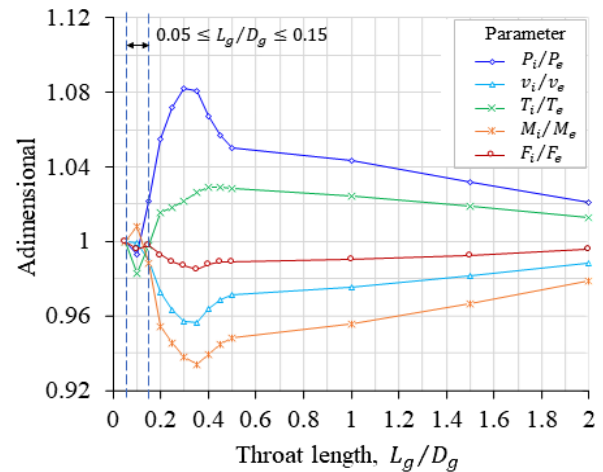| Parameters	Average values
Pressure: p_e (Pa)	69956.31
Velocity: v_e (m/s)	940.55
Temperature: T_e (K)	625.86
Mach number: M	1.873
Thrust force: F_e (N)	279.56

Figure 12. Curve trajectories of pressure, velocity, temperature, Mach number, and thrust force relationships for throat length range $0.05 \leq L_g/D_g \leq 2$.

Table 4: Standard deviation (SD) and coefficient of variation (CV) values for the thermodynamic flow parameters evaluated at the nozzle outlet.

	Range 1	Range 2	Range 3
Pressure ratio: p_i/p_e			
SD	0.01490	0.02525	0.02050
CV	1.482%	2.376%	1.951%
Velocity ratio: v_i/v_e			
SD	0.00562	0.01383	0.01063
CV	0.564%	1.428%	1.0931%
Temperature ratio: T_i/T_e			
SD	0.00942	0.01066	0.00624
CV	0.948%	1.049%	0.609%
Mach number ratio: M_i/M_e			
SD	0.00996	0.02179	0.01587
CV	0.996%	2.288%	1.665%
Thrust force ratio: F_i/F_e			
SD	0.0020	0.00507	0.00339
CV	0.200%	0.511%	0.342%

Of the conical nozzles studied, a throat section that is too long does not contribute significantly to improving the performance of the nozzle. On the contrary, Moreover, apart from originating a shock train, it also adds weight to its physical structure, which is not desirable. With respect to $L_g/D_g = 0.4$, suggested by Rogers [16], it should be addressed in future work for conical nozzles with longitudinal dimensions much larger than those studied in the present work in order to perform comparative studies of the flow behavior.

4. CONCLUSIONS

Based on the analyses of the numerical results obtained for the overexpanded flow condition for NPR = 12 in conical nozzles with throat length, applying CFD and simulating the flow turbulence with the ANSYS-Fluent R16.2 code that applies the FVM to discretize the computational domain, the following is concluded: The length of the throat section has a significant effect on the propagation of oblique waves; therefore, a shock train structure is configured as the straight-cut throat increases. The throat length $L_g/D_g = 0.15$ is an optimal range since the flow regime in the throat section does not exhibit flow fluctuations. Thus, the flow accelerates undisturbed. At the exit of the nozzle, the flow presents a higher velocity. Therefore, the thrust force is also higher. Whereas, for $L_g/D_g = 2$, the flow is accelerated and decelerated by the presence of the shock train and affects more strongly the flow regime in the divergent. For the range $0.15 < L_g/D_g \leq 2$, at the nozzle exit, the flow velocity decreases, as well as the thrust force. Therefore, it is evident that a straight-cut throat that is too long does not contribute significantly to the nozzle performance.

It should be noted that the numerical results obtained from the flow field in supersonic nozzles with straight-cut throats in the present work are related to several types of errors, such as modeling errors, discretization errors, iteration errors, programming, and user errors [26]. Therefore, it is considered pertinent in future work to perform laboratory experiments for straight-cut throat conical nozzle geometries for the overexpanded flow condition in order to correlate the numerical results with the experimental ones.

REFERENCES

[1] Matsuo, K. Miyazato, Y. and Kim, H.D.: Shock train and pseudo-shock phenomena in internal gas flows, Progress in Aerospace Sciences, Vol. 35, no. 1, pp. 33-100, 1999, https://doi.org/10.1016/s0376-0421(98)00011-6.

[2] Anderson, J.D.: *Hypersonic and high-temperature gas dynamics*, 3 ed., AIAA Education series: Blacksburg, Virginia, 2019.

[3] Sutton, G.P. and Biblarz, O.: *Rocket propulsion elements,* 9 ed., John Wiley and Sons: New York, 2016.

[4] Scarlatella, G. Tajmar, M. and Bach, C: Advanced nozzle concepts in retro-propulsion applications for reusable launch vehicle recovery: a case study, in:*72nd International Astronautical Congress (IAC),* Dubai, United Arab Emirates, 25-29 October, 2021, pp. 1-26.

[5] Carroll B.F. and Dutton, J.C: Characteristics of multiple shock wave/turbulent boundary-layer interactions in rectangular ducts, *Journal of Propulsion and Power*, Vol. 6, No. 2, pp. 186-193, 1990, https://doi.org/10.2514/3.23243.

[6] Gillespie, A. and Sandham, N.D: Numerical study of the effect of sidewalls on shock train behaviour, *flow,* 3, E12, pp. 1-19, 2023, https://doi.org/10.1017/flo.2023.6.

[7] Anderson, J.D: *Fundamentals of aerodynamics*, McGraw-Hill Education: New York, 2017.

[8] Schlichting, H. and Gersten, K.:*Boundary-layer theory*, 9 ed., Berlin Heidelberg, Germany, Springer Verlag, 2017.

[9] Östlund, J,. Muhammed-Klingmann, B.: Supersonic flow separation with application to rocket engine nozzles, *ASME, Applied Mechanics Reviews*, Vol. 58, No. 3, pp. 143–177, 2005, https://doi.org/10.1115/1.1894402.

[10] Hadjadj, A. Ben-Nasr, O., Shadloo, M.S. and Chaudhuri, A.: Effect of wall temperature in supersonic turbulent boundary layers: A numerical study, *International Journal of Heat and Mass Transfer,* Vol. 81, pp. 426-438, 2015, https://doi.org/10.1016/j.ijheatmasstransfer.2014.10.025.

[11] Zmijanović, V. Rašuo, B. and Chpoun, A.: Flow separation modes and side phenomena in an overexpanded nozzle, *FME Transactions*, Vol. 40, No. 3, pp. 111-118, 2012.

[12] Hirai R: and Kawai, S: Wall pressure fluctuations in wall heated and cooled shock wave and turbulent boundary layer interactions, *International Journal of heat and fluid flow*, Vol. 103, October, 2023, p. 109205, https://doi.org/10.1016/j.ijheatfluidflow.2023.109205.

[13] Hunter, C.A.: Experimental investigation of separated nozzle flows, *Journal of Propulsion and Power,* Vol. 20, No. 3, pp. 527-532, May-June, 2004, https://doi.org/10.2514/1.4612.

[14] Génin, C. Stark, R. and Karl, S.: Shock system deformation in high Mach number rocket nozzles, in:*Sasoh A., Aotki T., Katayama M. (eds)31st International Symposium on Shock Waves 2, ISSW 2017.* Springer, Cham., 2019, pp. 543-549, https://doi.org/10.1007/978-3-319-91017-8_69.

[15] Butal, P.V. and Uskov, V.N.:Mach reflection of a shock wave from the symmetry axis of the supersonic nonisobaric jet, *Research Journal of Applied Sciences, Engineering and Technology*, Vol. 8, No. 1, pp. 135–142. https://doi.org/10.19026/rjaset.8.951.

[16] Rogers, C.E.: The solid rocket motor-Part 4. Departures from ideal performance for conical nozzles and bell nozzles, straight-cut throats and rounded throats, *Tech series, High Power Rocketry magazine*, Orem, 2004.

[17] CRPCE-ULA: *ULA sounding rocket project*, http://www.ing.ula.ve/programaespacialula/Proyectos%20de%20Investigacion/PCSULA.html (in Spanish).

[18] Geerts, J.S. and Yu, K.H: Visualization of Shock Train-Boundary Layer Interaction in Mach 2.5 Isolator Flow, in:*43rd Fluid Dynamics Conference, AIAA 2013-3102,* 2013, pp. 1–13, https://doi.org/10.2514/6.2013-3102.

[19] Weiss, A. Grzona, A. and Olivier, H.: Behavior of shock trains in a diverging duct, *Experiments in Fluids*, Vol. 49, No. 2, pp. 355-365, 2010, https://doi.org/10.1007/s00348-009-0764-9.

[20] Arora, R. and Vaidyanathan, A. Experimental investigation of flow through planar double divergent nozzles, *Acta Astronautica*, Vol. 112, pp. 200-2016, 2015, https://doi.org/10.1016/j.actaastro.2015.03.020.

[21] Wang, Z. Chang, J. Wu, G. and Yu, D.: Experimental investigation of shock train behavior in a supersonic isolator, *Physics of Fluids*, Vol. 33, No. 4, 046103 1-26, 2021, https://doi.org/10.1063/5.0047665.

[22] Wang, C. Cheng, C. Cheng, K. and Xue, L.: Unsteady behavior of oblique shock train and boundary layer interactions, *Aerospace Science and Technology,* Vol. 79, pp. 212-222, 2018, https://doi.org/10.1016/j.ast.2018.05.054.

[23] Xue, L., Cheng, C. Wang, C. Zhang, L. Li, K.andCheng, K.: Oblique shock train motion based on schlieren image processing, *Chinese Journal of Aeronautics,* Vol. 36, No. 3, pp. 30-41, 2023, https://doi.org/10.1016/j.cja.2022.10.013.

[24] Fisher, C. and Olivier, H.: Experimental investigation of wall and total temperature influence on a shock train, *AIAA journal*, Vol. 52, No. 4, pp. 757-766, 2014, https://doi.org/10.2514/1.J052599.

[25] Blazek, j.: *Computational fluid dynamics: principles and applications*, Oxford, United Kingdom: Butterworth-Heinemann, 2015.

[26] Ferziger, J.H., Perić, M. and Street, R.L.: *Computational Methods for Fluid Dynamics*, 4 ed., Springer, 2020.

[27] Tolentino, S.L. Mírez, J. Caraballo, S.A.: Numerical analysis of the shock train evolution in planar nozzles with throat length, *FME Transactions*, Vol. 51, No. 4, pp. 595-605, 2023, https://doi.org/10.5937/fme2304595T.

[28] Tolentino, S.L. and Mírez, J.: Throat length effect on the flow patterns in off-design conical nozzles, *FME Transactions,* Vol. 50, No. 2, pp. 271-282, 2022, https://doi.org/10.5937/fme2201271T.

[29] Tolentino, S.L. Parco, M.A., Caraballo, S., Lacruz, L., Ferreira, J. and Mírez, J.:Numerical analysis of the flow behavior in the throat section of an experimental conical nozzle, *Journal Enfoque UTE*, Vol. 12, No. 1, pp. 12−28, 2021, (in Spanish), https://doi.org/10.29019/enfoqueute.676.

[30] Tolentino, S.L. and González, O.: Numerical analysis of the over-expanded flow in the experimental conical nozzle ULA-1B out of design, *Lámpsakos*, No 25, pp. 1-13, 2021, (in Spanish), https://doi.org/10.21501/21454086.3836.

[31] Tolentino, S.L. and Mírez, J.: Numerical analysis of over-expanded flow in the experimental ULA-2 conical nozzle out of design, *Lámpsakos*, No 24, pp. 33-47, 2020, (in Spanish), https://doi.org/10.21501/21454086.3707.

[32] ANSYS, Ansys Fluent 12.0 Theory guide. https://www.afs.enea.it/project/neptunius/docs/fluent/html/th/main_pre.htm

[33] Spalart, P.R: and Allmaras, S.R.: A one-equation turbulence model for aerodynamic flows, in:*30th Aerospace Sciences Meeting and Exhibit, 06 January 1992 – 09*, Reno, NV, U.S.A, 1992, pp. 1-22, https://doi.org/10.2514/6.1992-439.

[34] Sutherland, W.: The viscosity of gases and molecular force, *Philosophical Magazine series 5*, Vol. 36, No. 223, pp. 507–531, 1893.

[35] Menter, F.: Two equation eddy-viscosity Turbulence models for engineering applications, *AIAA Journal*, Vol. 32, pp. 1598-1605, 1994, https://doi.org/10.2514/3.12149.

[36] Wilcox, D.C.: Reassessment of the scale determining equation for advanced turbulence models, *AIAA Journal*, Vol. 26, No. 11, pp. 1299–1310, 1988, https://doi.org/10.2514/3.10041.

[37] Launder, B.E., Reece, G.J. and Rodi, W.: Progress in the development of a Reynolds-stress turbulence closure, *Journal of Fluid Mechanics,* Vol. 68, No. 3, pp. 537-566, 1975, https://doi.org/10.1017/s0022112075001814.

NOMENCLATURE

α	Half angle of the divergent
β	Half angle of the convergent
D_g	Throat diameter
L_c	Convergent length
L_g	Throat length
L_d	Divergent length
L_g/D_g	Straight-cut throat
M	Mach number
p_0	Stagnation pressure
p	Static pressure
R_g	Throat radius
T_0	Stagnation temperature
T	Static temperature
y^+	y-plus, in the shear stress value

НУМЕРИЧКА АНАЛИЗА УДАРНОГ ВОЗА У КОНУСНИМ МЛАЗНИЦАМА СА РАВНИМ ГРЛОМ

С.Л. Толентино, X. Мирес, С.А. Карабаљо

Прекомерно проширени режим струјања у млаз–ницама суперсоничног ракетног мотора представља различите структуре ударних таласа због геомет–ријске конфигурације унутрашњих зидова. У овом истраживању, проучавање феномена ударног влака је обрађено за групу конвергентно-дивергентних конусних млазница са равним изрезима за услов преоптерећеног струјања за NPR=12. Поље вискоз–ног и компресибилног струјања у стационарним условима симулирано је RANS моделом у ANS3S-Флуент P16.2 коду, који примењује метод коначних запремина (FVM) за дискретизацију рачунарског домена. Коришћен је Спаларт-Аллмарасов модел

турбуленције, а Сатерлендов закон је коришћен за вискозитет као функцију температуре. Резултати показују да се у одсеку грла правог пресека, како се његова дужина повећава, проток убрзава и успорава уз присуство косих удара, што формира дефи–

нитивну структуру ударног влака, где су флук–туације брзине струјања унутар процењеног опсега Маховог броја. од 0,6 до 1,8. Повећање дужине грла значајно утиче на развој протока на излазу млазнице, чиме се смањује сила потиска.